



# G9a promotes muscular atrophy in chronic aging and acute denervation

Ying Jin<sup>1†</sup>, Wei Kang<sup>1†</sup>, Xiaoge Ji<sup>1</sup>, Yihao Zhou<sup>1</sup> and Ling Zheng<sup>1\*</sup>

## Abstract

Muscular atrophy accompanied by neuromuscular junction (NMJ) denervation is often observed after long-term chronic diseases and aging and is associated with substantial morbidity and mortality. Here, we report that histone methyltransferase G9a is elevated in the muscle of muscular atrophy model mice and that muscle-specific deficiency of G9a (*Ehmt2*<sup>Ckmm-KO</sup>) alleviates muscular atrophy in both aged and denervated mice. Moreover, increased nerve-to-myofiber ratios and increased Agrin-Lrp4-MuSK signaling, which maintains NMJ, are found in aged *Ehmt2*<sup>Ckmm-KO</sup> mice. Together, these data suggest that G9a promotes muscular atrophy and disrupts NMJ; thus, inhibiting the G9a level may be a potential therapy for muscular atrophy.

**Keywords** Muscular atrophy, Neuromuscular junctions, Aging, Denervation, G9a

## Introduction

Skeletal muscle is a crucial organ for physical activity and exercise, and it also serves as a metabolic locus that regulates body homeostasis (Jin et al. 2023). As the largest protein reservoir of the body, skeletal muscle accounts for 40%-50% of the body weight of mammals (Kettelhut et al. 1988). Normally, there is dynamic homeostasis for skeletal muscle protein synthesis and degradation (Zhang et al. 2024); however, protein degradation may exceed synthesis under some physiological or pathological conditions, such as aging, denervation, lack of exercise, or diseases, which reduce muscle mass, strength and function, a status defined as muscular atrophy (Sartori et al. 2021; Lan et al. 2024).

Currently, muscular atrophy has attracted increasing attention because of its deleterious impacts on quality of life and increased mortality (Sayer et al. 2022, Coletta and Phillips 2023). In humans, the prevalence of muscular atrophy is 11%-18% in the elderly population (Fernandes et al. 2022), 0.63%-7.22% in obese individuals (Hu et al. 2024), and 30%-80% in cancer patients (Tisdale 2009), and no effective medication is currently available (Rolland and Cruz-Jentoft 2023). In animal husbandry, muscular atrophy compromises meat production efficiency and results in enormous economic losses. Muscle RING-finger protein-1 (MuRF1; encoded by *Trim63*) and muscle atrophy F-Box protein (Atrogin-1; encoded by *Fbxo32*) are well-known muscular atrophy biomarkers, and their deletion mitigates muscular atrophy in mouse models (Bodine et al. 2001; Gomes et al. 2001; Yin et al. 2021).

The neuromuscular junction (NMJ) is composed of a presynaptic membrane (cell membrane of the motor neuron terminal), a synaptic cleft and a postsynaptic membrane (myofiber membrane). When electrical signals reach motor neurons, the neurotransmitter acetylcholine (ACh) is released from the presynaptic membrane and bound to its receptor (AChR) on the postsynaptic membrane to complete

Handling Editor: Caihua Dong.

<sup>†</sup>Ying Jin and Wei Kang contributed equally to this work.

\*Correspondence:

Ling Zheng

lzheng@whu.edu.cn

<sup>1</sup> Hubei Key Laboratory of Cell Homeostasis, Frontier Science Center for Immunology and Metabolism, College of Life Sciences, Wuhan University, Wuhan 430072, China



© The Author(s) 2024. **Open Access** This article is licensed under a Creative Commons Attribution 4.0 International License, which permits use, sharing, adaptation, distribution and reproduction in any medium or format, as long as you give appropriate credit to the original author(s) and the source, provide a link to the Creative Commons licence, and indicate if changes were made. The images or other third party material in this article are included in the article's Creative Commons licence, unless indicated otherwise in a credit line to the material. If material is not included in the article's Creative Commons licence and your intended use is not permitted by statutory regulation or exceeds the permitted use, you will need to obtain permission directly from the copyright holder. To view a copy of this licence, visit <http://creativecommons.org/licenses/by/4.0/>. The Creative Commons Public Domain Dedication waiver (<http://creativecommons.org/publicdomain/zero/1.0/>) applies to the data made available in this article, unless otherwise stated in a credit line to the data.

signal transmission from motor neurons to muscle fibers. NMJ morphology varies considerably in health and disease. In healthy adults, NMJs are "pretzel-like", with complete overlap of the presynaptic membrane and the postsynaptic membrane, suggesting that the muscle fibers are fully innervated. Under disease conditions, the presynaptic membrane and the synaptic membrane disappear; moreover, the number of AchRs on the postsynaptic membrane and their binding affinity are reduced, suggesting that muscle fibers undergo denervation (Pratt et al. 2021).

The cluster of AchRs on the postsynaptic membrane of NMJs is regulated by Agrin-Lrp4 (low-density lipoprotein receptor-related protein 4)-MuSK (muscle-specific receptor tyrosine kinase) signaling. Lrp4 and MuSK are located on the postsynaptic membrane. After Agrin is secreted by motor neurons, it binds to Lrp4, which enhances MuSK activation and further promotes AchR clustering on the postsynaptic membrane (Zhang et al. 2008; Yumoto et al. 2012). Disruption of the agrin-Lrp4-MuSK signaling pathway causes an abnormal cluster of AchRs, which leads to NMJ dysfunction and ultimately muscular atrophy (Kostrominova et al. 2022). Therefore, maintaining the NMJ structure may represent an important strategy for treating muscular atrophy.

Recently, alterations in DNA methylation and histone acetylation have been shown to play important roles in muscular atrophy, whereas no histone methylation has been identified (Livshits and Kalinkovich 2024). G9a (encoded by *Ehmt2*) is a histone H3K9me1/2 methyltransferase that plays crucial roles in embryonic development (Tachibana et al. 2002) and muscle function maintenance, including myocyte differentiation and metabolic homeostasis (Ling et al. 2012; Zhang et al. 2020a). In addition, G9a also regulates neuronal development, cardiac development, tumorigenesis (Poulard et al. 2021), and liver and kidney injury (Zhang et al. 2020b; Yang et al. 2023b). However, its role in muscular atrophy remains unclear.

Here, we used aging and sciatic nerve denervation mouse models to explore the role of muscular G9a in muscular atrophy under physiological and pathological conditions. We found that muscular G9a was elevated in aging or sciatic nerve-denervated mice. Aged skeletal muscle-specific G9a knockout (*Ehmt2*<sup>Ckmm</sup> KO) mice presented mitigated muscular atrophy and superior exercise performance, with significantly upregulated NMJ maintenance-related genes and signaling, as well as a greater innervation ratio in myofibers. Moreover, G9a knockout alleviated sciatic nerve denervation-induced muscular atrophy. Our work thus reveals a deleterious role of G9a in muscular atrophy.

## Results

### G9a is significantly upregulated in the skeletal muscle of aged male mice

To investigate whether the G9a level is altered in the skeletal muscle of aged mice, the mRNA and protein levels of G9a in the tibialis anterior (TA) muscle of young (5–6-month-old) and aged (18–24-month-old) mice were examined. Compared with that of young mice, the transcriptional level of *Ehmt2* was significantly increased 4.1-fold, whereas its protein level was significantly elevated 5.7-fold in aged mice (Fig. 1A–C). Immunofluorescence staining further revealed an increased number of G9a<sup>+</sup>-stained nuclei in the TA muscle of aged mice (Fig. 1D–E). Elevated G9a in aging skeletal muscle may play a role in the development of age-induced muscular atrophy.

### Muscle-specific knockout of G9a improves the exercise capacity of aged mice

To investigate the role of G9a in age-induced muscular atrophy, we constructed muscle-specific knockout G9a (*Ehmt2*<sup>Ckmm</sup> KO) mice (Fig. S1A–B). Since locomotor performance is one of the most sensitive indicators of skeletal muscle strength, while loss of locomotor performance is associated with age-induced muscular atrophy (Damluji et al. 2023), the running locomotor performance of young and aged WT and *Ehmt2*<sup>Ckmm</sup> KO male mice was examined. Compared with aged WT mice, aged *Ehmt2*<sup>Ckmm</sup> KO mice presented significant increases in running distance and running time (Fig. 2A–B), whereas young WT and *Ehmt2*<sup>Ckmm</sup> KO mice presented similar running capacities under the same protocol (Fig. 2A–B), suggesting that skeletal muscle G9a may reduce exercise capacity and contribute to aging-associated muscular atrophy.

The better running performance may be due to increased muscle force; thus, we examined the muscle force of young and aged WT and *Ehmt2*<sup>Ckmm</sup>-KO mice via in situ analysis. However, the tetanic force in the TA of *Ehmt2*<sup>Ckmm</sup> KO mice was significantly greater than that in the TA of aged WT mice under 80–160 Hz electrical stimulus in both the young and aged groups (Fig. 2C–D), and the maximal tetanic force of *Ehmt2*<sup>Ckmm</sup> KO mice was significantly greater than that of WT mice under optimal 100 Hz electrical stimulation in both the young and aged groups (Fig. 2C–D). These results suggest that skeletal muscle G9a may affect muscle strength before aging.

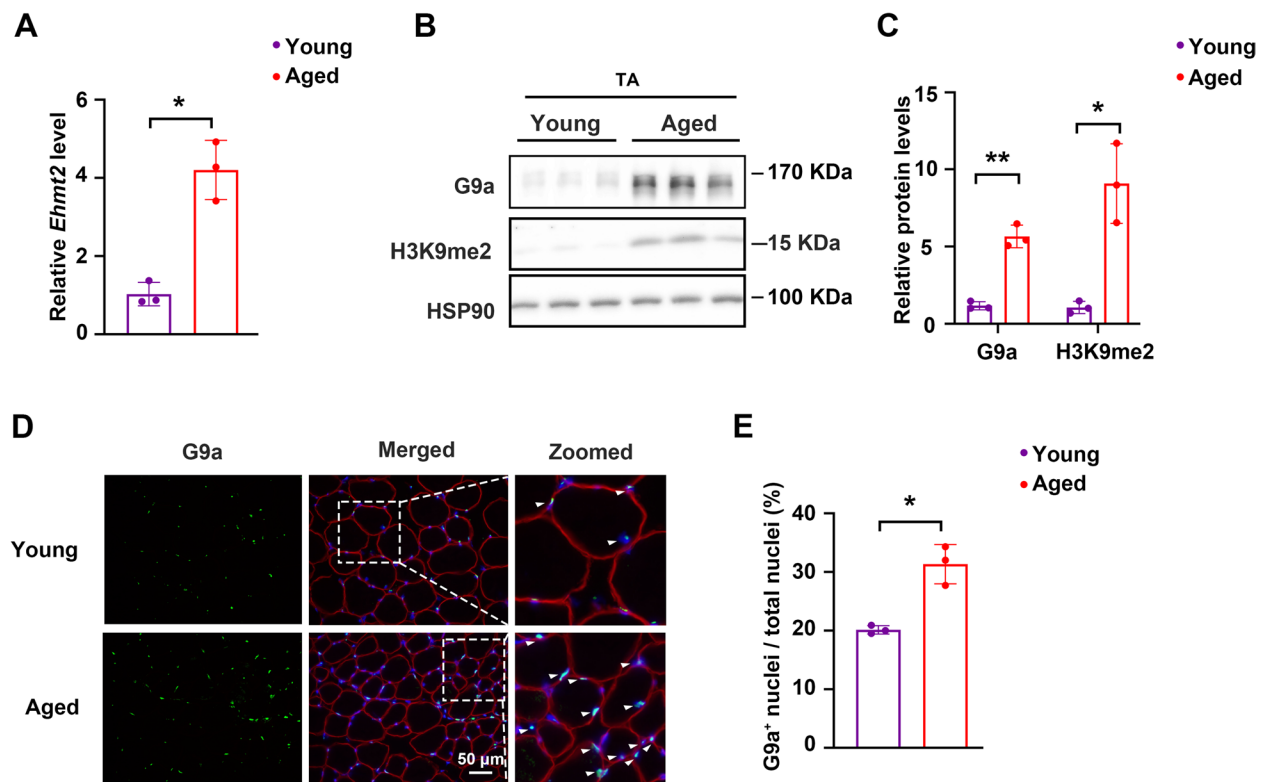


**Fig. 1** The G9a expression level is significantly increased in the skeletal muscle of aged mice. **A** qPCR results of *Ehmt2* in the TAs of young and aged mice. **B–C** Western blots of G9a (**B**) and quantitative analysis (**C**) of the TAs of young and aged mice. **D–E** Representative images of G9a immunostaining (**D**) and quantitative analysis (**E**) of the TAs of young and aged mice; green, positive G9a staining; red, positive laminin staining; blue, DAPI-stained nuclei. TA, tibialis anterior; young, 5–6 months old; aged, 18–24 months old;  $n = 3$  per group; \* $P < 0.05$ , \*\* $P < 0.01$

### Muscle-specific knockout of G9a alleviates muscular atrophy in aged mice

Compared with those of young WT mice, smaller myofiber diameters and a reduced cross-sectional area (CSA) of muscle fibers were found in the TA muscle of aged WT mice (Figure S2A–B), which is consistent with aged-induced muscular atrophy indicated by muscle fiber degeneration and CSA reduction (Burden et al. 2013). We addressed whether muscle-specific knockout of G9a affects aged-induced muscular atrophy. Although no significant difference in body weight was detected between WT and *Ehmt2*<sup>Ckmm</sup> KO mice at the young or aged stage (Fig. 3A), increased weights of the gastrocnemius (Gastroc) and TA muscles, but not the extensor digitorum longus (EDL) and soleus muscles, were detected in *Ehmt2*<sup>Ckmm</sup> KO mice even when the weights were normalized to the corresponding body weights (Fig. 3B). However, there were no significant differences in muscle weight between young WT and *Ehmt2*<sup>Ckmm</sup>-KO mice (Fig. S3). H&E staining revealed that aged *Ehmt2*<sup>Ckmm</sup> mice had larger muscle fiber cross-sectional areas in the TA region (Fig. 3C). Furthermore, a significantly increased average

cross-sectional area, due to a decreased proportion of small muscle fibers and an increased proportion of large muscle fibers, was found in aged *Ehmt2*<sup>Ckmm</sup>-KO mice (Fig. 3C). The mRNA levels of *Trim63* (encoding MuRF1) and *Fbxo32* (encoding Atrogin-1), two well-known muscular atrophy-related genes (Yin et al. 2021), were significantly reduced in the TA muscle of aged *Ehmt2*<sup>Ckmm</sup>-KO mice (Fig. 3D). Moreover, *Trim63*, but not *Fbxo32*, was significantly reduced in the TA muscle of young *Ehmt2*<sup>Ckmm</sup>-KO mice (Fig. 3D). Consistently, the protein levels of MuRF1 and Atrogin-1 were also significantly reduced in the TA muscle of aged *Ehmt2*<sup>Ckmm</sup>-KO mice, whereas only MuRF1 was significantly reduced in that of young *Ehmt2*<sup>Ckmm</sup>-KO mice (Fig. 3E). Together, these results suggest that muscular atrophy is mitigated in aged *Ehmt2*<sup>Ckmm</sup> KO mice.

### Muscle-specific knockout of G9a improves NMJ maintenance in aged mice

To further investigate the role of G9a in aging-induced muscular atrophy, RNA-seq analysis was performed on the TAs of aged WT and *Ehmt2*<sup>Ckmm</sup>-KO mice. KEGG pathway analysis revealed significantly upregulated

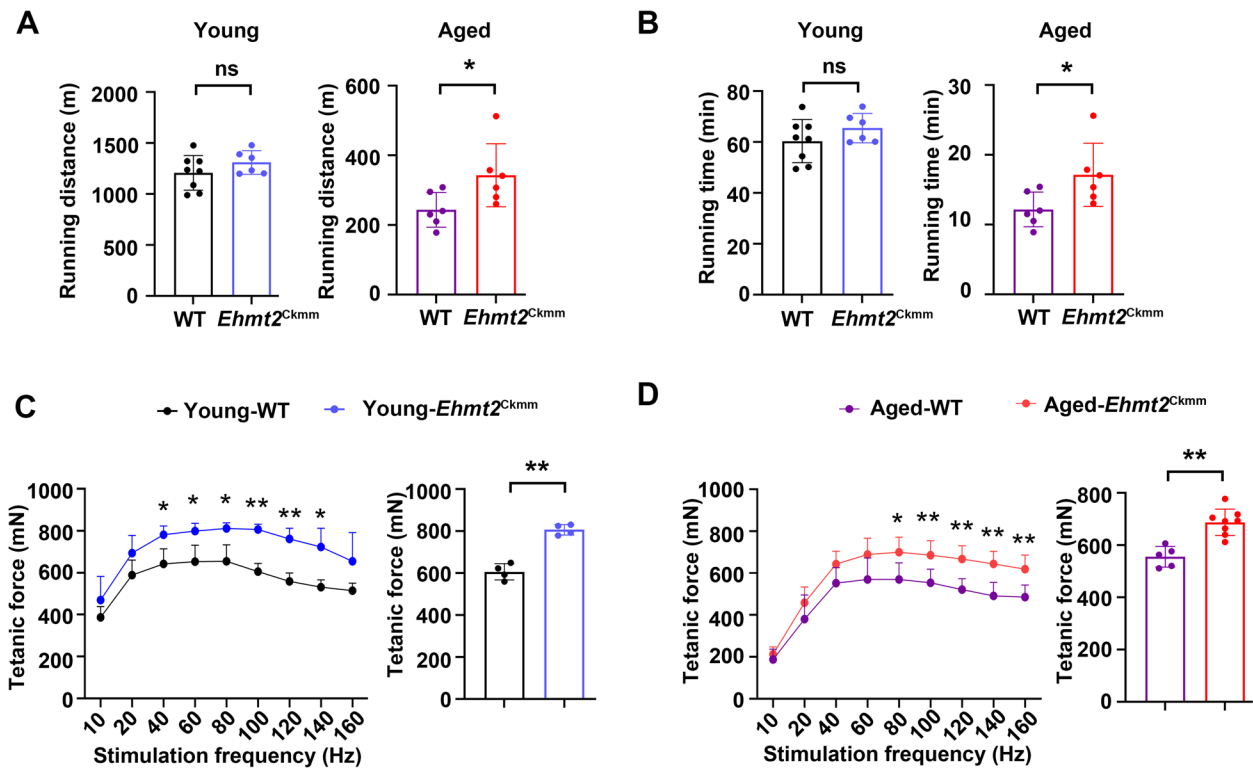


**Fig. 2** Muscle-specific knockout of G9a improves exercise capacity in aged mice. **A** Running distance of young (left) and aged (right) WT and *Ehmt2<sup>Ckmm</sup>* KO mice subjected to treadmill exercise. **B** Running time of young (left) and aged (right) WT and *Ehmt2<sup>Ckmm</sup>* KO mice subjected to treadmill exercise. **C** Maximum tetanic force of the TA in young WT and *Ehmt2<sup>Ckmm</sup>*-KO mice under different frequencies of electrical stimulation (left) and 100 Hz electrical stimulation (right). **D** Maximum tetanic force of the TA in aged WT and *Ehmt2<sup>Ckmm</sup>*-KO mice under different frequencies of electrical stimulation (left) and 100 Hz electrical stimulation (right). TA, tibialis anterior; *n* = 4–8 per group; ns, no significant difference; \**P* < 0.05, \*\**P* < 0.01

cholinergic synapse and serotonergic synapse signaling pathways in aged *Ehmt2<sup>Ckmm</sup>*-KO mice (Fig. 4A). Heatmap and qPCR verification demonstrated that cholinergic synapse-related genes, including *Gng11* (G protein subunit gamma 1) and *Gnao1* (G protein subunit alpha O1), as well as serotonergic synapse-related genes, including *Lrtm1* (leucine-rich repeats and transmembrane domains 1) and *Maob* (monoamine oxidase B), were significantly increased in aged *Ehmt2<sup>Ckmm</sup>*-KO mice (Fig. 4B-C). Next, we found that neuromuscular junction-associated genes were enriched through Gene Ontology (GO) analysis (Fig. 4D), and key factors involved in AchR clustering (Tintignac et al. 2015), such as cholinergic receptor nicotinic beta 1 subunit (*Chrn1*) and the cholinergic receptor nicotinic epsilon subunit (*Chrne*), were also upregulated (Fig. 4E). Furthermore, GO analysis revealed that *Musk*, the key gene for NMJ maintenance, was upregulated (Fig. 5A), and Agrin-Lrp4-MusK and its downstream signaling factors, including *Agrin*, *Musk*, *Rapsyn* (receptor-associated protein of the synapse) and *App* (amyloid beta precursor protein) (Li et al. 2018), were upregulated (Fig. 5B). We next stained

NMJs by labeling the postsynaptic membrane with  $\alpha$ -bungarotoxin ( $\alpha$ -BTX) and the presynaptic membrane with anti-synaptophysin and anti-neurofilament antibodies. The results revealed that aged *Ehmt2<sup>Ckmm</sup>* KO mice were more innervated than were aged WT mice (Fig. 5C-D). These results suggest that G9a may affect muscular atrophy by modulating NMJ maintenance.

**G9a is significantly upregulated in denervation-induced muscular atrophy in mice**

We next examined whether G9a also responds to muscular atrophy under pathological conditions. Sciatic nerve transection was performed on 12-week-old C57BL/6 male mice. The successful establishment of the denervation-induced mouse muscular atrophy model was demonstrated by lower Gastroc, TA and soleus muscle weights and a smaller cross-sectional area of the TA in the denervated mice (Fig. S4A-B). Compared with those in the sham-operated side, significantly increased *Ehmt2* levels and muscular atrophy-related gene (*Trim63* and *Fbxo32*) levels were detected in the TA region of the denervated side (Fig. S4C). Moreover,

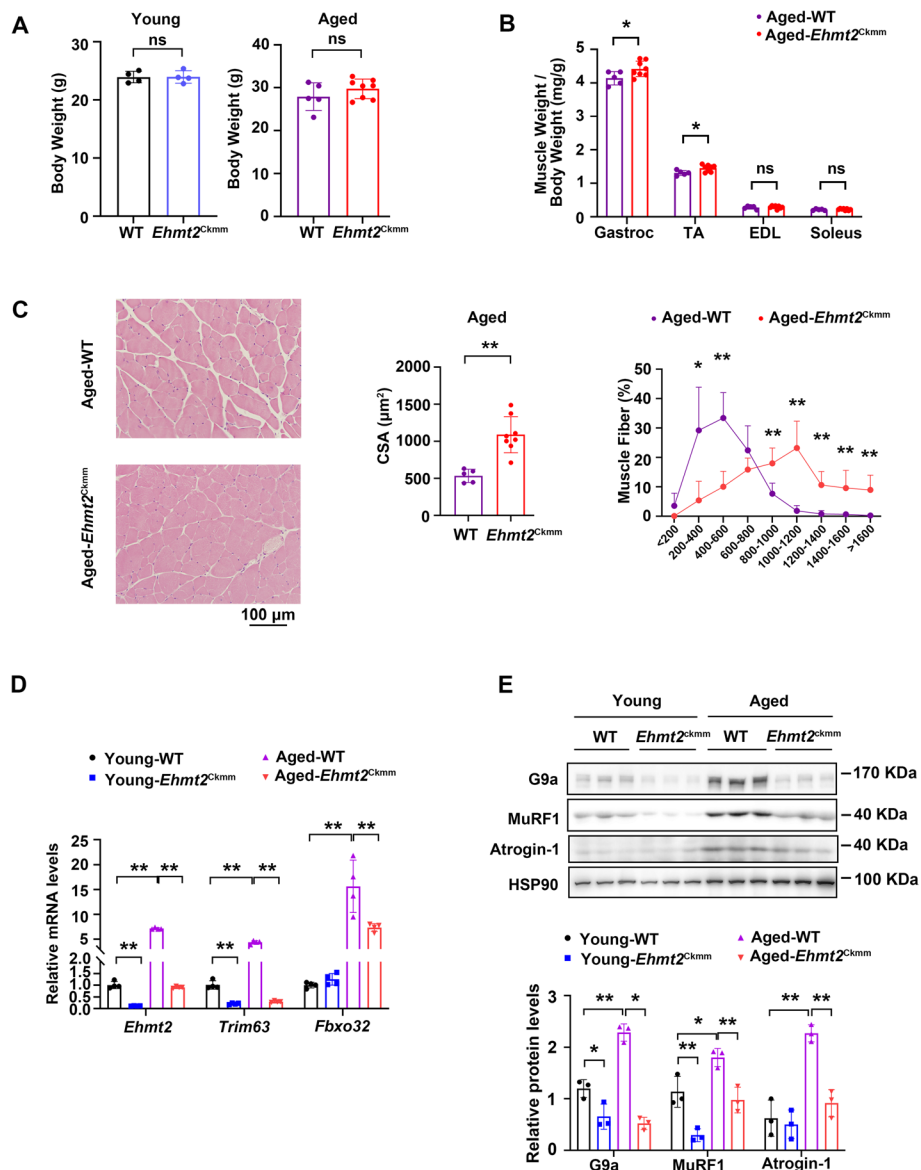


**Fig. 3** Muscle-specific knockout of G9a alleviates muscular atrophy in aged mice. **A** Body weights of young (left) and aged (right) WT and *Ehmt2<sup>Ckmm</sup>* KO mice. **B** Quantification of the skeletal muscle weight/body weight ratio in aged WT and *Ehmt2<sup>Ckmm</sup>*-KO mice. **C** Representative images of H&E staining (left), average (middle) and distribution (right) of myofiber CSA in the TAs of aged WT and *Ehmt2<sup>Ckmm</sup>* KO mice. **D** qPCR results of *Ehmt2* and muscular atrophy genes (*Trim63* and *Fbxo32*) in the TAs of young and aged WT and *Ehmt2<sup>Ckmm</sup>* KO mice. **E** Western blots (up) with quantitative results (bottom) of G9a and muscular atrophy markers (MuRF1 and Atrogin-1) in the TAs of young and aged WT and *Ehmt2<sup>Ckmm</sup>*-KO mice. Gastroc, gastrocnemius; TA, tibialis anterior; EDL, extensor digitorum longus; CSA, cross-sectional area;  $n = 3-8$  per group; ns, no significant difference,  $*P < 0.05$ ,  $**P < 0.01$

increased MuRF1, Atrogin-1, and G9a levels were also detected on the denervated side compared with those on the sham-operated side (Fig. S4D). Immunofluorescence experiments further revealed more G9a-positive nuclei in the TA on the denervated side than on the sham-operated side (Fig. S4E). These data suggest that G9a may also play an important role in denervation-induced muscular atrophy.

**Muscle-specific knockout of G9a mitigates denervation-induced muscular atrophy**

To further investigate the role of G9a in denervation-induced muscular atrophy, WT and *Ehmt2<sup>Ckmm</sup>*-KO mice were subjected to skeletal muscle denervation. There was no significant difference in the weights of the Gastroc, TA, EDL or soleus between WT and *Ehmt2<sup>Ckmm</sup>*-KO mice on the denervated side and those

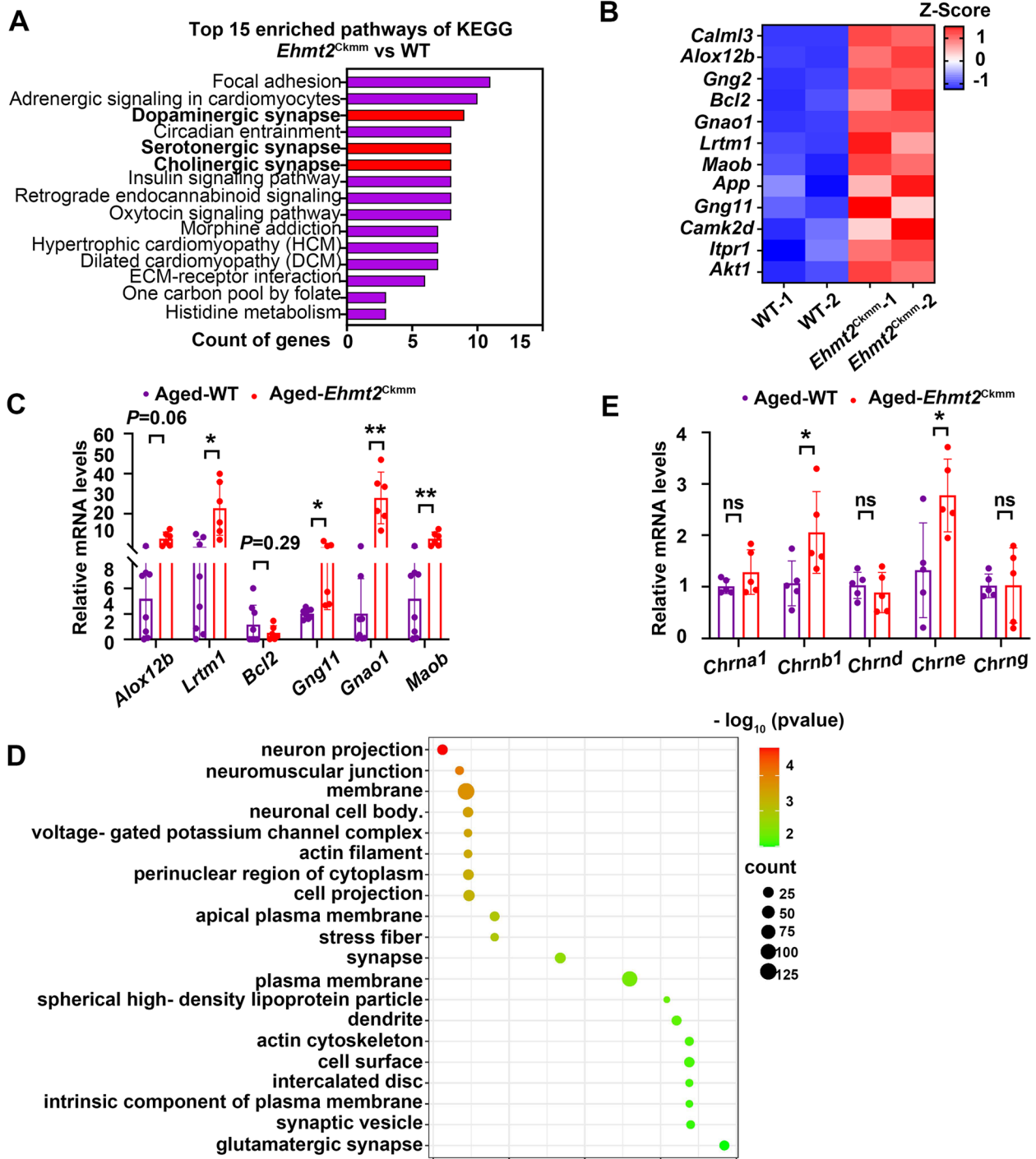


**Fig. 4** Muscle-specific knockout of G9a improves NMJ-associated gene expression in aged mice. **A** KEGG pathway analysis of the 15 pathways enriched in the RNA sequencing data of TAs from aged WT and *Ehmt2*<sup>Ckmm</sup>-KO mice. **B-C** Differentially expressed genes associated with synapse formation in the TA of aged WT and *Ehmt2*<sup>Ckmm</sup>-KO mice are shown as heatmaps (**B**) and qPCR results (**C**). **D** Gene Ontology (GO) enrichment analysis of gene transcripts in the TAs of aged WT and *Ehmt2*<sup>Ckmm</sup>-KO mice. **E** qPCR results of AChR subunits. AChR, acetylcholine receptor; TA, tibialis anterior; *n*=5–8 per group; ns, no significant difference; \**P*<0.05, \*\**P*<0.01

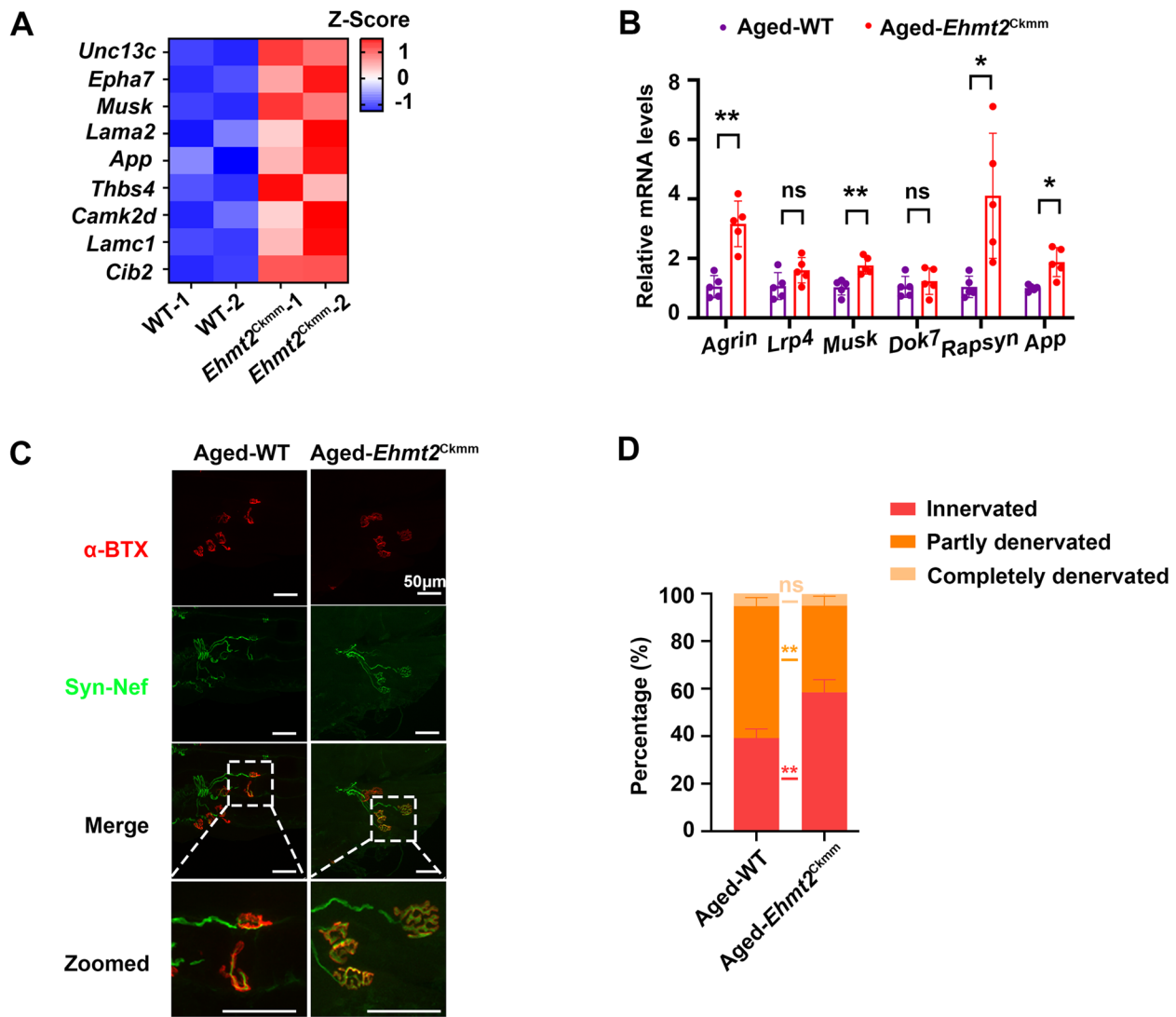


**Fig. 5** Muscle-specific knockout of G9a improves NMJ maintenance in aged mice. **A-B** Heatmap (**A**) and qPCR results (**B**) of genes involved in neuromuscular junction formation and maintenance in the TA of aged WT and *Ehmt2<sup>Ckmm</sup>* KO mice. **C** Immunofluorescence staining of NMJs in the TAs of aged WT and *Ehmt2<sup>Ckmm</sup>*-KO mice. **D** Percentages of innervated myofibers in the TAs of aged WT and *Ehmt2<sup>Ckmm</sup>*-KO mice. Syn, Synaptophysin (green); Nef, Neurofilament (green);  $\alpha$ -BTX,  $\alpha$ -Bungarotoxin (red); TA, tibialis anterior;  $n = 3-5$  per group; ns, no significant difference,  $*P < 0.05$ ,  $**P < 0.01$

on the sham-operated side at 14 days after injury (Fig. S5). The CSA of the TA myofibers on the denervated side was greater in the *Ehmt2<sup>Ckmm</sup>*-KO mice than in the WT mice (Fig. 6A). Furthermore, qPCR and immunoblotting analyses revealed that the mRNA level of *Trim63* and the protein level of MuRF1 were significantly lower in the TA muscle of the denervated side of *Ehmt2<sup>Ckmm</sup>* KO mice than in that of the denervated WT mice (Fig. 6B-C), suggesting that muscle-specific knockdown of G9a slowed muscular atrophy.

**Discussion**

Epigenetic alterations are involved in muscular atrophy. The DNA methyltransferase DNMT3a (DNA methyltransferase 3a) and histone deacetylases such as HDAC1 (histone deacetylase 1), HDAC6 (histone deacetylase 6), Sirt1 (sirtuin 1) and Sirt2 (sirtuin 2) have been reported to regulate muscular atrophy (Shen and He 2021, Han et al. 2021; Beharry et al. 2014; Zhong et al. 2023; Ratti et al. 2015). In some congenital myopathies, epigenetic changes are considered common inducers of muscle weakness, and HDAC and DNA methyltransferase

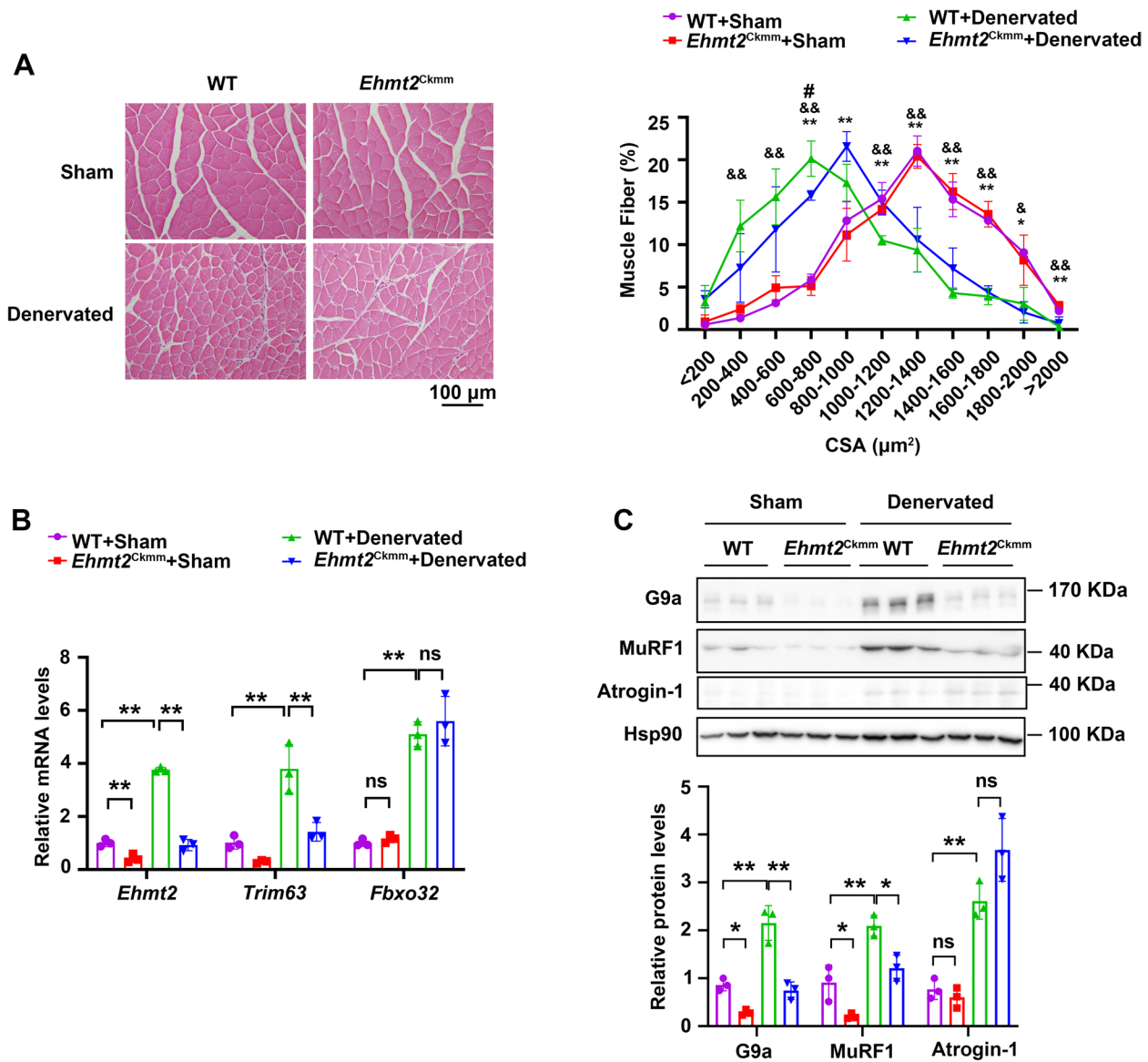


**Fig. 6** Muscle-specific knockout of G9a mitigates denervation-induced muscular atrophy. **A** Representative H&E staining (left) showing the distribution of myofiber CSA (right) in the TAs of sham-operated or denervated WT and *Ehmt2<sup>Ckmm</sup>* KO mice. **B** qPCR results of *Ehmt2*, *Trim63* and *Fbxo32* in the TA of sham-operated or denervated WT and *Ehmt2<sup>Ckmm</sup>* KO mice. **C** Western blots (top) and quantitative results (bottom) of G9a, MuRF1 and Atrogin-1 expression in the TAs of sham-operated or denervated WT and *Ehmt2<sup>Ckmm</sup>*-KO mice. TA, tibialis anterior; *n* = 3 per group; (A): WT + Sham vs WT + Denervated, \**P* < 0.05, &#P < 0.01; *Ehmt2<sup>Ckmm</sup>* + Sham vs *Ehmt2<sup>Ckmm</sup>* + Denervated, \**P* < 0.05, \*\**P* < 0.01; WT + Denervated vs *Ehmt2<sup>Ckmm</sup>* + Denervated, #*P* < 0.05; (B–C): ns, no significant difference, \**P* < 0.05, \*\**P* < 0.01

inhibitors have been shown to ameliorate congenital myopathy (Ruiz et al. 2022, Volpatti et al. 2022, Livshits and Kalinkovich 2024). An epigenome-wide association study revealed differential methylation at 176 dmCpGs (differentially methylated CpG sites) and 141 differentially methylated regions between age-related sarcopenic and control individuals (Antoun et al. 2022). Overall, epigenetic modifications, including methylation, have been shown to impact muscular atrophy, but the role of

histone methyltransferases remains unclear. Here, we found that histone methyltransferase G9a was significantly upregulated in the muscles of muscular atrophy model mice (Figs. 1–6), indicating that G9a may participate in muscular atrophy.

G9a is essential for development; G9a-knockout embryos exhibit delayed development and early death on embryonic day 9.5 (Tachibana et al. 2002), and neuron-specific deletion of G9a results in defects in cognition and

adaptive behaviors (Poulard et al. 2021). Moreover, G9a plays a crucial role in myogenesis, and G9a inhibits myoblast differentiation through the methylation of MyoD (myogenic differentiation) at Lys104 (Ling et al. 2012) and of MEF2D (myocyte enhancer factor 2D) at Lys26 in vitro (Zhang et al. 2016). In vivo, global inhibition of G9a enzyme activity promoted muscle regeneration (Biferali et al. 2021), whereas *Ehmt2<sup>floxex</sup> Myod<sup>cre</sup>* (*Ehmt2<sup>ΔmyoD</sup>*) mice presented normal skeletal muscle development (Zhang et al. 2016), possibly because myogenesis is a complicated process coordinated by multiple cell types, and G9a expressed in cell types other than myocytes also contributes. In this work, we show that G9a exacerbates muscular atrophy in both the aging model and denervation models (Figs. 3 and 6). However, no alteration in the mRNA level of *MyoD*, the key myogenic regulatory factor (Park et al. 2017), was found in RNA-sequencing data from aged WT and *Ehmt2<sup>Ckmm</sup>*-KO mice (data not shown), indicating similar self-repair capacity in these aged mice.

Interestingly, fewer denervated myofibers were observed in aged *Ehmt2<sup>Ckmm</sup>*-KO mice than in WT mice, suggesting that G9a may regulate muscular atrophy through cross talk between muscles and nerves. In skeletal muscle, NMJ links the nervous system and the muscular system (Yadav and Dabur 2024). Myofiber denervation is a hallmark of muscle dysfunction, which leads to decreased muscle function and muscular atrophy diseases such as aging-related sarcopenia, amyotrophic lateral sclerosis (ALS) and spinal muscular atrophy (SMA) (Fish and Fallon 2020). Mounting evidence indicates that epigenetic alterations are involved in the maintenance of NMJ function. For example, the DNA methylation profiles of patients with myasthenia gravis suggest that differences in methylation sites are associated with NMJ dysfunction (Lin et al. 2023). In addition, overexpression of the DNA methyltransferase DNMT3a alleviates skeletal muscular atrophy caused by denervation (Tajrishi et al. 2014). The overexpression of the histone deacetylase Sirt1 in motor neurons protects NMJs from aging and ALS (Herskovits et al. 2018). Here, NMJ maintenance signaling was significantly upregulated in aged *Ehmt2<sup>Ckmm</sup>*-KO mice (Figs. 4 and 5). Thus, using two models of muscular atrophy caused by aging and pathological denervation, we found that G9a exacerbates muscular atrophy under physiological and pathological conditions, possibly by affecting the maintenance of NMJs.

## Conclusion

In conclusion, this study revealed elevated G9a levels in the muscles of muscularly atrophied mice. Muscle-specific deletion of G9a alleviated muscular atrophy in both

the aging model and sciatic nerve injury model. G9a may disrupt NMJ maintenance to aggravate muscular atrophy. These findings may provide a new angle for muscular atrophy treatment.

## Methods

### Animals

*Ehmt2<sup>flox/flox</sup>* mice and *Ckmm-Cre* mice on a C57BL/6 background were used to generate muscle-specific G9a *Ehmt2<sup>Ckmm</sup>*-KO mice as we previously reported (Zhang et al. 2020a, b). The mice were maintained in a specific-pathogen-free, temperature-controlled (22°C ± 1°C) animal facility with a 12-h light/dark cycle and free access to water and food. Only male mice were used in the present study. The animals were handled according to the Guidelines of the China Animal Welfare Legislation, as approved by the Committee on Ethics in the Care and Use of Laboratory Animals of the College of Life Sciences, Wuhan University.

### Aging mouse model

Eighteen- to twenty-four-month-old WT and *Ehmt2<sup>Ckmm</sup>* KO mice were used for the aging experiments, whereas 5- to 6-month-old WT and *Ehmt2<sup>Ckmm</sup>* mice were used as young controls.

### Sciatic nerve transection mouse model

Three-month-old WT and *Ehmt2<sup>Ckmm</sup>* KO mice were used. The mice were anesthetized, and then the left sciatic nerve was bluntly exposed. A sciatic nerve transection model was established through a transection 0.3 cm distal to the sciatic notch. For the sham operation, the right sciatic nerve was exposed without transection. Muscle tissues were collected at 14 d after injury.

### Treadmill exercise

After 3 d of adaptive treadmill training (5 m/min, 20 min, -5° downhill), the weight of the mouse was recorded, and the mouse was warmed at 5 m/min and -5° downhill for 10 min. Then, the treadmill speed was gradually increased to 20 m/min with an acceleration speed of 2 m/min. The mouse was kept on the treadmill at a speed of 20 m/min until exhausted (it no longer ran even under continuous electric shock for 10 times). The total running time and running distance for each mouse were recorded from the beginning to the end of the experiment.

### In situ muscle function analysis

The tibialis anterior (TA) muscle was subjected to in situ muscle contractile function assessments via the Whole Animal System (Aurora Scientific 1300A, Aurora, ON) as previously reported (Ahn et al. 2022). Briefly, a small incision near the ankle was made to uncover the TA muscle

after anesthesia. The TA muscle was detached from the tibia while it was linked to the force probe on the distal side via a surgical suture and to the knee region on the proximal side. The platform was adjusted to ensure that the probe was in line with the knee, and two needle electrodes were placed, one at the distal end of the TA and the other under the kneecap near the sciatic nerve. The muscle was stimulated at 10 mA by two needle electrodes, and tetanic contractions were first measured by 500 ms stimuli and a 0.2 ms pulse width at a series of frequencies from 10 to 160 Hz (10, 20, 40, 60, 80, 100, 120, 140 and 160 Hz) with an interval of 1 min. Then, the muscle was stimulated at a single frequency under the optimal electrical stimulation conditions (100 Hz) to obtain the maximal tetanic contraction force.

#### RNA extraction and quantitative real-time PCR (qPCR)

RNA extraction and qPCR were performed as previously described (Wang et al. 2022a; Chen et al. 2022; Huang et al. 2022). Briefly, RNA was isolated from tissues via RNAiso Plus (Takara Biotech, Dalian, China). Two milligrams of RNA from each sample was reverse transcribed into cDNA via M-MLV (Thermo Fisher Scientific, Waltham, MA). qPCR was performed via target-specific primers (Supplementary Table 1) and SYBR Green probes (Yeasen Biotech, Shanghai, China). Relative transcript levels were calculated via the comparative CT method, and *Rn18s* was used as the internal control.

#### RNA sequencing

Total RNA from the TA muscle of WT and *Ehmt2*<sup>Ckmm</sup> KO mice was isolated individually. Equal amounts of RNA (n=6) from the same group were combined into two samples/group for RNA-seq. Sequencing and data analysis were performed by Novogene Bioinformatics (Beijing, China) as we previously reported (Yuan et al. 2023, Fan et al. 2023, Wang et al. 2022b).

#### Western blots

TA muscle was homogenized with RIPA buffer (Beyotime, Shanghai, China) supplemented with protease inhibitors and phosphatase inhibitors (Millipore, Billerica, MA). A total of 20–50 mg of protein per sample was separated via SDS-PAGE and electroblotted onto a PVDF membrane (Millipore, Billerica, MA). The membranes were incubated with primary antibodies (Supplementary Table 2) overnight, after which the blots were incubated with the appropriate HRP-conjugated secondary antibodies (Bio-Rad, Hercules, CA) (Supplementary Table 2). The targeted protein bands were visualized with enhanced chemiluminescence reagent (Beyotime) and evaluated via Quantity One (V. 4.6.2) as previously

described (Chen et al. 2023; Xiong et al. 2023; Yang et al. 2023a).

#### Muscle histology and immunohistochemical and immunofluorescence staining

Some of the TA muscles were fixed in 4% paraformaldehyde, embedded in paraffin, sectioned, and stained with hematoxylin and eosin (H&E) to analyze the mouse skeletal muscle cross-sectional area (CSA), whereas some were embedded in Tissue-Tek OCT (Tissue Tek, Torrance, CA) for cryosectioning. For each section, 3–6 fields of view were randomly selected, and pictures were taken. The distribution of myofiber cross-sectional areas was manually distinguished and counted via Image-Pro Plus 6.0.

For G9a and laminin immunofluorescence staining, primary antibodies were applied to cryosections (Supplementary Table 2) overnight at 4°C. The sections were then incubated with the corresponding secondary antibodies (both from Thermo Fisher Scientific, Waltham, MA) (Supplementary Table 2), followed by DAPI staining. The number of G9a-positive cells was directly analyzed via Image-Pro Plus 6.0 (Media Cybernetics, Rockville, MD).

For NMJ immunofluorescence staining, flash-frozen muscles were sectioned at 40 μm (longitudinal sections). The sections were fixed with 4% paraformaldehyde and then incubated with 0.2% Triton X-100. After the samples were blocked and stained with combined primary antibodies (anti-synaptophysin (Syn) plus anti-neurofilament (Nef)) (Supplementary Table 2) to label presynaptic parts at 4°C overnight, they were incubated with AlexaFluor 647-labeled a-bungarotoxin (Thermo Fisher Scientific) to label postsynaptic parts (mostly AChRs), as well as the corresponding Alexa Fluor 488-conjugated secondary antibodies (both from Thermo Fisher Scientific) (Supplementary Table 2), for 2 h at room temperature. Images were taken under a Leica TCS SP8 confocal microscope (Leica, Germany). Image-pro plus 6.0 software (Media Cybernetics, Rockville, MD) was used to quantify the structure of the NMJs. 'Overlap' is defined as the congruence of the pre- and postsynaptic parts of the NMJ and is scored as complete denervation (overlap < 20%), partial denervation (20% < overlap < 90%) or innervation (overlap > 90%) for the NMJ with the formula  $\text{overlap} = (\text{total area AChRs-unoccupied area AChRs}) / \text{total area AChRs} * 100\%$ , as reported (Jones et al. 2016).

#### Statistical analysis

All the results are expressed as the mean ± S.D. (standard deviation). The sample size (n) for each experimental group is indicated in the figure legends. All the statistical analyses were performed via GraphPad Prism 8 (La Jolla, San Diego, CA). When the data were

normally distributed, an unpaired, two-tailed Student's *t* test was used for two-group comparisons, whereas 1-way ANOVA with Tukey's multiple-comparison test was used for multiple-group comparisons.  $P < 0.05$  was considered statistically significant.

#### Abbreviations

MuRF1	Muscle RING-finger protein-1
Atrogin-1	Muscle atrophy F-Box protein
NMJ	Neuromuscular junction
Ach	Acetylcholine
AchR	Acetylcholine receptor
Lrp4	Low-density lipoprotein receptor-related protein 4
MuSK	Muscle-specific receptor tyrosine kinase
qPCR	Quantitative real-time PCR
CSA	Cross-sectional area
Syn	Synaptophysin
Nef	Neurofilament
S.D.	Standard deviation
TA	Tibialis anterior
Gastroc	Gastrocnemius
EDL	Extensor digitorum longus
<i>Bcl2</i>	B-cell lymphoma 2
<i>Gng11</i>	G protein subunit gamma
<i>Gnao1</i>	G protein subunit alpha O1
<i>Alox12b</i>	Arachidonate 12-lipoxygenase, 12R type
<i>Lrtm1</i>	Leucine-rich repeats and transmembrane domains 1
<i>Maob</i>	Monoamine oxidase B
<i>Chrn1</i>	Cholinergic receptor nicotinic beta 1 subunit
<i>Chrne</i>	Cholinergic receptor nicotinic epsilon subunit
GO	Gene Ontology
<i>Rapsyn</i>	Receptor-associated protein of the synapse
<i>App</i>	Amyloid beta precursor protein
$\alpha$ -BTX	$\alpha$ -Bungarotoxin
DNMT3a	DNA methyltransferase 3a
HDAC1	Histone Deacetylase 1
HDAC6	Histone Deacetylase 6
Sirt1	Sirtuin 1
Sirt2	Sirtuin 2
dmCpGs	Differentially methylated CpG sites
MyoD	Myogenic differentiation
MEF2D	Myocyte enhancer factor 2D
ALS	Amyotrophic lateral sclerosis
SMA	Spinal muscular atrophy

#### Supplementary Information

The online version contains supplementary material available at <https://doi.org/10.1186/s44149-024-00147-6>.

Supplementary Material 1.

#### Acknowledgements

The authors would like to thank Prof. Bin Zhang (School of Basic Medical Science, Tongji Medical College, Huazhong University of Science and Technology) for the NMJ staining protocols and helpful suggestions on the work.

#### Authors' contributions

Y.J., W.K. and L.Z. designed the study and analyzed the data. Y.J., W.K., X.J. and Y.Z. performed the experiments. W.K., Y.J., X.J. and L.Z. wrote the manuscript.

#### Funding

This work is supported by the Natural Science Foundation of China (32271222).

#### Data availability

Data will be made available upon reasonable request.

#### Declarations

##### Ethics approval and consent to participate

The animals were handled according to the Guidelines of the China Animal Welfare Legislation, as approved by the Committee on Ethics in the Care and Use of Laboratory Animals of the College of Life Sciences, Wuhan University.

##### Consent for publication

All the authors approved and provided their consent for publication of the manuscript.

##### Competing interests

The authors declare that they have no competing interests.

Received: 26 July 2024 Accepted: 20 October 2024

Published online: 05 November 2024

#### References

- Ahn, B., R. Ranjit, P. Kneis, H. Xu, K. M. Piekarz, W. M. Freeman, M. Kinter, A. Richardson, Q. Ran, S. V. Brooks, et al. 2022. Scavenging mitochondrial hydrogen peroxide by peroxiredoxin 3 overexpression attenuates contractile dysfunction and muscle atrophy in a murine model of accelerated sarcopenia. *Aging Cell* 21 (3): e13569. <https://doi.org/10.1111/accel.13569>.
- Antoun, E., E. S. Garratt, A. Taddei, M. A. Burton, S. J. Barton, P. Titcombe, L. D. Westbury, A. Baczynska, E. Migliavacca, J. N. Feige, et al. 2022. Epigenome-wide association study of sarcopenia: Findings from the Hertfordshire Sarcopenia Study (HSS). *Journal of Cachexia, Sarcopenia and Muscle* 13 (1): 240–253. <https://doi.org/10.1002/jcsm.12876>.
- Beharry, A. W., P. B. Sandesara, B. M. Roberts, L. F. Ferreira, S. M. Senf, and A. R. Judge. 2014. HDAC1 activates FoxO and is both sufficient and required for skeletal muscle atrophy. *Journal of Cell Science* 127 (Pt 7): 1441–1453. <https://doi.org/10.1242/jcs.136390>.
- Biferali, B., V. Bianconi, D. F. Perez, S. P. Kronawitter, F. Marullo, R. Maggio, T. Santini, F. Polverino, S. Biagioni, V. Summa, et al. 2021. Prdm16-mediated H3K9 methylation controls fibro-adipogenic progenitors identity during skeletal muscle repair. *Science Advances* 7 (23). <https://doi.org/10.1126/sciadv.abd9371>.
- Bodine, S. C., E. Latres, S. Baumhueter, V. K. Lai, L. Nunez, B. A. Clarke, W. T. Poueymirou, F. J. Panaro, E. Na, K. Dharmarajan, et al. 2001. Identification of ubiquitin ligases required for skeletal muscle atrophy. *Science* 294 (5547): 1704–1708. <https://doi.org/10.1126/science.1065874>.
- Burden, S. J., N. Yumoto, and W. Zhang. 2013. The role of MuSK in synapse formation and neuromuscular disease. *Cold Spring Harbor Perspectives in Biology* 5 (5): a009167. <https://doi.org/10.1101/cshperspect.a009167>.
- Chen, H., C. Liu, Q. Wang, M. Xiong, X. Zeng, D. Yang, Y. Xie, H. Su, Y. Zhang, Y. Huang, et al. 2022. Renal UTX-PHGDH-serine axis regulates metabolic disorders in the kidney and liver. *Nature Communications* 13 (1): 3835. <https://doi.org/10.1038/s41467-022-31476-0>.
- Chen, Y., J. Shi, X. Wang, L. Zhou, Q. Wang, Y. Xie, C. Peng, L. Kuang, D. Yang, J. Yang, et al. 2023. An antioxidant feedforward cycle coordinated by linker histone variant H1.2 and NRF2 that drives non-small cell lung cancer progression. *Proceedings of the National Academy of Sciences* 120 (39): e2306288120. <https://doi.org/10.1073/pnas.2306288120>.
- Coletta, G., and S. M. Phillips. 2023. An elusive consensus definition of sarcopenia impedes research and clinical treatment: A narrative review. *Ageing Research Reviews* 86: 101883. <https://doi.org/10.1016/j.arr.2023.101883>.
- Damluji, A. A., M. Alfaraidhy, N. AlHajri, N. N. Rohant, M. Kumar, C. Al Malouf, S. Bahrainy, M. Ji Kwak, W. B. Batchelor, D. E. Forman, et al. 2023. Sarcopenia and cardiovascular diseases. *Circulation* 147 (20): 1534–1553. <https://doi.org/10.1161/circulationaha.123.064071>.
- Fan, Y., Y. Yuan, M. Xiong, M. Jin, D. Zhang, D. Yang, C. Liu, R. B. Petersen, K. Huang, A. Peng, et al. 2023. Tet1 deficiency exacerbates oxidative stress in acute kidney injury by regulating superoxide dismutase. *Theranostics* 13 (15): 5348–5364. <https://doi.org/10.7150/thno.87416>.
- Fernandes, L. V., A. E. G. Paiva, A. C. B. Silva, I. C. de Castro, A. F. Santiago, E. P. de Oliveira, and L. C. J. Porto. 2022. Prevalence of sarcopenia according

- to EWGSOP1 and EWGSOP2 in older adults and their associations with unfavorable health outcomes: A systematic review. *Aging Clinical and Experimental Research* 34 (3): 505–514. <https://doi.org/10.1007/s40520-021-01951-7>.
- Fish, L. A., and J. R. Fallon. 2020. Multiple MuSK signaling pathways and the aging neuromuscular junction. *Neuroscience Letters* 731: 135014. <https://doi.org/10.1016/j.neulet.2020.135014>.
- Gomes, M. D., S. H. Lecker, R. T. Jague, A. Navon, and A. L. Goldberg. 2001. Atrogin-1, a muscle-specific F-box protein highly expressed during muscle atrophy. *Proceedings of the National Academy of Sciences USA* 98 (25): 14440–14445. <https://doi.org/10.1073/pnas.251541198>.
- Han, Z., C. Chang, W. Zhu, Y. Zhang, J. Zheng, X. Kang, G. Jin, and Z. Gong. 2021. Role of SIRT2 in regulating the dexamethasone-activated autophagy pathway in skeletal muscle atrophy. *Biochemistry and Cell Biology* 99 (5): 562–569. <https://doi.org/10.1139/bcb-2020-0445>.
- Herskovits, A. Z., T. A. Hunter, N. Maxwell, K. Pereira, C. A. Whittaker, G. Valdez, and L. P. Guarente. 2018. SIRT1 deacetylase in aging-induced neuromuscular degeneration and amyotrophic lateral sclerosis. *Aging Cell* 17 (6): e12839. <https://doi.org/10.1111/acel.12839>.
- Hu, F., G. Zhang, Z. Xu, Z. Zuo, N. Huang, M. Ge, X. Liu, and B. Dong. 2024. The diagnostic agreement of sarcopenic obesity with different definitions in Chinese community-dwelling middle-aged and older adults. *Frontiers in Public Health* 12: 1356878. <https://doi.org/10.3389/fpubh.2024.1356878>.
- Huang, Y., Y. Xie, D. Yang, M. Xiong, X. Chen, D. Wu, Q. Wang, H. Chen, L. Zheng, and K. Huang. 2022. Histone demethylase UTX aggravates acetaminophen overdose induced hepatotoxicity through dual mechanisms. *Pharmacological Research* 175: 106021. <https://doi.org/10.1016/j.phrs.2021.106021>.
- Jin, L., S. Han, X. Lv, X. Li, Z. Zhang, H. Kuang, Z. Chen, C. A. Lv, W. Peng, Z. Yang, et al. 2023. The muscle-enriched myokine Musclin impairs beige fat thermogenesis and systemic energy homeostasis via Tfr1/PKA signaling in male mice. *Nature Communications* 14 (1): 4257. <https://doi.org/10.1038/s41467-023-39710-z>.
- Jones, R. A., C. D. Reich, K. N. Dissanayake, F. Kristmundsdottir, G. S. Findlater, R. R. Ribchester, M. W. Simmen, and T. H. Gillingwater. 2016. NMJ-morph reveals principal components of synaptic morphology influencing structure-function relationships at the neuromuscular junction. *Open Biology* 6 (12). <https://doi.org/10.1098/rsob.160240>.
- Kettelhut, I. C., S. S. Wing, and A. L. Goldberg. 1988. Endocrine regulation of protein breakdown in skeletal muscle. *Diabetes/metabolism Reviews* 4 (8): 751–772. <https://doi.org/10.1002/dmr.5610040805>.
- Kostrominova, T. Y. 2022. Skeletal muscle denervation: Past, present and future. *International Journal of Molecular Sciences* 23 (14). <https://doi.org/10.3390/ijms23147489>.
- Lan, X. Q., C. J. Deng, Q. Q. Wang, L. M. Zhao, B. W. Jiao, and Y. Xiang. 2024. The role of TGF- $\beta$  signaling in muscle atrophy, sarcopenia and cancer cachexia. *General and Comparative Endocrinology* 353: 114513. <https://doi.org/10.1016/j.ygcen.2024.114513>.
- Li, L., W. C. Xiong, and L. Mei. 2018. Neuromuscular junction formation, aging, and disorders. *Annual Review of Physiology* 80: 159–188. <https://doi.org/10.1146/annurev-physiol-022516-034255>.
- Lin, J., L. Tao, L. Deng, R. Zhou, S. Lou, S. Chen, X. Chen, C. Lu, P. Li, and B. Hu. 2023. Epigenome-wide DNA methylation analysis of myasthenia gravis. *FEBS Open Bio* 13 (7): 1375–1389. <https://doi.org/10.1002/2211-5463.13656>.
- Ling, B. M., N. Bharathy, T. K. Chung, W. K. Kok, S. Li, Y. H. Tan, V. K. Rao, S. Gopinadhan, V. Sartorelli, M. J. Walsh, et al. 2012. Lysine methyltransferase G9a methylates the transcription factor MyoD and regulates skeletal muscle differentiation. *Proceedings of the National Academy of Sciences & U S A* 109 (3): 841–846. <https://doi.org/10.1073/pnas.1111628109>.
- Livshits, G., and A. Kalinkovich. 2024. Restoration of epigenetic impairment in the skeletal muscle and chronic inflammation resolution as a therapeutic approach in sarcopenia. *Ageing Research Reviews* 96: 102267. <https://doi.org/10.1016/j.arr.2024.102267>.
- Park, S. S., E. S. Kwon, and K. S. Kwon. 2017. Molecular mechanisms and therapeutic interventions in sarcopenia. *Osteoporos Sarcopenia* 3 (3): 117–122. <https://doi.org/10.1016/j.afos.2017.08.098>.
- Poulard, C., L. M. Noureddine, L. Pruvost, and M. Le Romancer. 2021. Structure, activity, and function of the protein lysine methyltransferase G9a. *Life (Basel)* 11 (10). <https://doi.org/10.3390/life11101082>.
- Pratt, J., G. De Vito, M. Narici, and C. Boreham. 2021. Neuromuscular junction aging: a role for biomarkers and exercise. *Journals of Gerontology. Series a, Biological Sciences and Medical Sciences* 76 (4): 576–585. <https://doi.org/10.1093/gerona/glaa207>.
- Ratti, F., F. Ramond, V. Moncollin, T. Simonet, G. Milan, A. Méjat, J.L. Thomas, N. Streichenberger, B. Gilquin, P. Matthias, et al. 2015. Histone deacetylase 6 is a FoxO transcription factor-dependent effector in skeletal muscle atrophy. *Journal of Biological Chemistry* 290 (7): 4215–4224. <https://doi.org/10.1074/jbc.M114.600916>.
- Rolland, Y., and A. J. Cruz-Jentoft. 2023. Editorial: Sarcopenia: Keeping on search for the best operational definition. *The Journal of Nutrition, Health & Aging* 27 (3): 202–204. <https://doi.org/10.1007/s12603-023-1099-1>.
- Ruiz, Alexis, Sofia Benucci, Urs Duthaler, Christoph Bachmann, Martina Franchini, Faiza Noreen, Laura Pietrangolo, Feliciano Protasi, Susan Treves, and Francesco Zorzato. 2022. Improvement of muscle strength in a mouse model for congenital myopathy treated with HDAC and DNA methyltransferase inhibitors. *eLife* 11: e73718. <https://doi.org/10.7554/eLife.73718>.
- Sartori, R., V. Romanello, and M. Sandri. 2021. Mechanisms of muscle atrophy and hypertrophy: Implications in health and disease. *Nature Communications* 12 (1): 330. <https://doi.org/10.1038/s41467-020-20123-1>.
- Sayer, A. A., and A. Cruz-Jentoft. 2022. Sarcopenia definition, diagnosis and treatment: consensus is growing. *Age Ageing* 51 (10). <https://doi.org/10.1093/aging/afac220>.
- Shen, D., and Z. He. 2021. Mesenchymal stem cell-derived exosomes regulate the polarization and inflammatory response of macrophages via miR-21-5p to promote repair after myocardial reperfusion injury. *Annals of Translational Medicine* 9 (16): 1323. <https://doi.org/10.21037/atm-21-3557>.
- Tachibana, M., K. Sugimoto, M. Nozaki, J. Ueda, T. Ohta, M. Ohki, M. Fukuda, N. Takeda, H. Niida, H. Kato, et al. 2002. G9a histone methyltransferase plays a dominant role in euchromatic histone H3 lysine 9 methylation and is essential for early embryogenesis. *Genes & Development* 16 (14): 1779–1791. <https://doi.org/10.1101/gad.989402>.
- Tajrishi, M. M., J. Shin, M. Hetman, and A. Kumar. 2014. DNA methyltransferase 3a and mitogen-activated protein kinase signaling regulate the expression of fibroblast growth factor-inducible 14 (Fn14) during denervation-induced skeletal muscle atrophy. *Journal of Biological Chemistry* 289 (29): 19985–19999. <https://doi.org/10.1074/jbc.M114.568626>.
- Tintignac, L. A., H. R. Brenner, and M. A. Rüegg. 2015. Mechanisms regulating neuromuscular junction development and function and causes of muscle wasting. *Physiological Reviews* 95 (3): 809–852. <https://doi.org/10.1152/physrev.00033.2014>.
- Tisdale, M. J. 2009. Mechanisms of cancer cachexia. *Physiological Reviews* 89 (2): 381–410. <https://doi.org/10.1152/physrev.00016.2008>.
- Volpatti, Jonathan R., Mehdi M. Ghahramani-Seno, Mélanie. Mansat, Nesrin Sabha, Ege Sarikaya, Sarah J. Goodman, Eric Chater-Diehl, Alper Celik, Emanuela Pannia, Carine Froment, et al. 2022. X-linked myotubular myopathy is associated with epigenetic alterations and is ameliorated by HDAC inhibition. *Acta Neuropathologica* 144 (3): 537–563. <https://doi.org/10.1007/s00401-022-02468-7>.
- Wang, J., M. Xiong, Y. Fan, C. Liu, Q. Wang, D. Yang, Y. Yuan, Y. Huang, S. Wang, Y. Zhang, et al. 2022a. MeCP2 protects kidney from ischemia-reperfusion injury through transcriptional repressing IL-6/STAT3 signaling. *Theranostics* 12 (8): 3896–3910. <https://doi.org/10.7150/thno.72515>.
- Wang, Q., Y. Chen, Y. Xie, D. Yang, Y. Sun, Y. Yuan, H. Chen, Y. Zhang, K. Huang, and L. Zheng. 2022b. Histone H1.2 promotes hepatocarcinogenesis by regulating signal transducer and activator of transcription 3 signaling. *Cancer Science* 113 (5): 1679–1692. <https://doi.org/10.1111/cas.15336>.
- Xiong, M., H. Chen, Y. Fan, M. Jin, D. Yang, Y. Chen, Y. Zhang, R. B. Petersen, H. Su, A. Peng, et al. 2023. Tubular Elabela-APJ axis attenuates ischemia-reperfusion induced acute kidney injury and the following AKI-CKD transition by protecting renal microcirculation. *Theranostics* 13 (10): 3387–3401. <https://doi.org/10.7150/thno.84308>.
- Yadav, A., and R. Dabur. 2024. Skeletal muscle atrophy after sciatic nerve damage: Mechanistic insights. *European Journal of Pharmacology* 970: 176506. <https://doi.org/10.1016/j.ejphar.2024.176506>.
- Yang, C., H. Xu, D. Yang, Y. Xie, M. Xiong, Y. Fan, X. Liu, Y. Zhang, Y. Xiao, Y. Chen, et al. 2023a. A renal YY1-KIM1-DR5 axis regulates the progression of acute kidney injury. *Nature Communications* 14 (1): 4261. <https://doi.org/10.1038/s41467-023-40036-z>.

- Yang, D., Y. Fan, M. Xiong, Y. Chen, Y. Zhou, X. Liu, Y. Yuan, Q. Wang, Y. Zhang, R. B. Petersen, et al. 2023b. Loss of renal tubular G9a benefits acute kidney injury by lowering focal lipid accumulation via CES1. *EMBO Reports* 24 (6): e56128. <https://doi.org/10.15252/embr.202256128>.
- Yin, L., N. Li, W. Jia, N. Wang, M. Liang, X. Yang, and G. Du. 2021. Skeletal muscle atrophy: From mechanisms to treatments. *Pharmacological Research* 172: 105807. <https://doi.org/10.1016/j.phrs.2021.105807>.
- Yuan, Y., Y. Fan, Y. Zhou, R. Qiu, W. Kang, Y. Liu, Y. Chen, C. Wang, J. Shi, C. Liu, et al. 2023. Linker histone variant H1.2 is a brake on white adipose tissue browning. *Nature Communications* 14 (1): 3982. <https://doi.org/10.1038/s41467-023-39713-w>.
- Yumoto, N., N. Kim, and S. J. Burden. 2012. Lrp4 is a retrograde signal for presynaptic differentiation at neuromuscular synapses. *Nature* 489 (7416): 438–442. <https://doi.org/10.1038/nature11348>.
- Zhang, B., S. Luo, Q. Wang, T. Suzuki, W. C. Xiong, and L. Mei. 2008. LRP4 serves as a coreceptor of agrin. *Neuron* 60 (2): 285–297. <https://doi.org/10.1016/j.neuron.2008.10.006>.
- Zhang, R. H., R. N. Judson, D. Y. Liu, J. Kast, and F. M. Rossi. 2016. The lysine methyltransferase Ehmt2/G9a is dispensable for skeletal muscle development and regeneration. *Skeletal Muscle* 6: 22. <https://doi.org/10.1186/s13395-016-0093-7>.
- Zhang, W., D. Yang, Y. Yuan, C. Liu, H. Chen, Y. Zhang, Q. Wang, R. B. Petersen, K. Huang, and L. Zheng. 2020a. Muscular G9a regulates muscle-liver-fat axis by musclin under overnutrition in female mice. *Diabetes* 69 (12): 2642–2654. <https://doi.org/10.2337/db20-0437>.
- Zhang, Y., W. Xue, W. Zhang, Y. Yuan, X. Zhu, Q. Wang, Y. Wei, D. Yang, C. Yang, Y. Chen, et al. 2020b. Histone methyltransferase G9a protects against acute liver injury through GSTP1. *Cell Death and Differentiation* 27 (4): 1243–1258. <https://doi.org/10.1038/s41418-019-0412-8>.
- Zhang, H. J., B. H. Wang, X. Wang, C. P. Huang, S. M. Xu, J. L. Wang, T. E. Huang, W. L. Xiao, X. L. Tian, X. Q. Lan, et al. 2024. Handelin alleviates cachexia- and aging-induced skeletal muscle atrophy by improving protein homeostasis and inhibiting inflammation. *Journal of Cachexia, Sarcopenia and Muscle* 15 (1): 173–188. <https://doi.org/10.1002/jcsm.13381>.
- Zhong, Q., K. Zheng, W. Li, K. An, Y. Liu, X. Xiao, S. Hai, B. Dong, S. Li, Z. An, et al. 2023. Posttranslational regulation of muscle growth, muscle aging and sarcopenia. *Journal of Cachexia, Sarcopenia and Muscle* 14 (3): 1212–1227. <https://doi.org/10.1002/jcsm.13241>.

## Publisher's Note

Springer Nature remains neutral with regard to jurisdictional claims in published maps and institutional affiliations.